First-principles study of compensation mechanisms in negatively charged LaGaO_{3}/MgAl_{2}O_{4} interfaces

Alejandro Rébola, Dillon D. Fong, Jeffrey A. Eastman, Serdar Öğüt, and Peter Zapol

Phys. Rev. B **87**, 245117 — Published 18 June 2013

DOI: 10.1103/PhysRevB.87.245117

First-principles study of compensation mechanisms in negatively charged $LaGaO_3/MgAl_2O_4$ interfaces

Alejandro Rébola,[1,2] Dillon D. Fong,[2] Jeffrey A. Eastman,[2] Serdar Öğüt,[1] and Peter Zapol[2*]

[1] *Department of Physics, University of Illinois at Chicago, Chicago, IL 60607, USA,*

[2] *Materials Science Division, Argonne National Laboratory, Argonne, IL 60439 USA*

Abstract

Thin film oxide heterostructures with a bound charge at the interface require electrical compensation, which can involve redistribution of mobile charge carriers. We explore a model $LaGaO_3(001)//MgAl_2O_4(001)$ heterostructure with nominally negatively charged interfaces using first-principles methods and a Poisson-Boltzmann equation. We find that charge compensation by oxygen vacancies with quadratically decaying concentration away from the interface is more favorable than electronic redistribution. These vacancies have a potential to enhance ionic conductivity along the interfaces.

PACS numbers: 68.35.bg, 68.35.Dv,66.30.H-,68.35.Fx

I. INTRODUCTION

The fascinating and diverse electrical properties of thin film heterostructures have drawn worldwide attention in recent years.[1–4] The physical origins of this diversity are inherent to the interfacial structures and include symmetry-breaking and epitaxial strain. In turn, the resulting changes in the charge distribution and crystal field can drive atomic relaxations and reconstructions, creating a much larger manifold of possible structures and, consequently, electrical properties compared to parent bulk structures. In particular, interfacial ion transport has been widely investigated in oxide materials. Higher mobility at temperatures below 800°C would have a profound impact on applications in energy conversion devices.[5] Many undoped bulk materials have good mobilities but a limited number of carriers. In many cases, despite the fact that it is possible to increase the number of charged carriers by doping, interactions between dopant ions and their charge-compensating defects lead to the formation of distinct clusters that decrease the mobilities of the migrating species.[6] Some interfaces in oxides are known to enhance ionic diffusion.[7–9] Modifications of interfacial charge to manipulate properties of the space charge layer provide another venue of changing transport properties in the proximity of an interface. If the density of the interfaces is such that space charge layers overlap, one can expect emergent behavior of ionic transport properties that cannot be interpolated from the bulk counterpart behavior. However, it is well known that grain boundaries in acceptor-doped oxide perovskites[1] and fluorites[2] are typically positively charged relative to the bulk. This leads to oxygen vacancy depletion layers, and a consequent reduction in ionic conduction. For heterostructures with oxygen vacancies as the dominant carriers, a possible route to enhance in-plane interfacial ionic transport is to induce oxygen vacancy enrichment in space charge layers during synthesis. Here, we describe a computational study of such a thin film heterostructure.

Heterogeneous doping is a well-known strategy for enhancing ionic conductivity by increasing the concentration of mobile point defects in the vicinity of the interface (i.e., in the space charge region).[3] Heterolayers were also demonstrated to significantly improve ionic conductivity in CaF_2/BaF_2 superlattices, with conductivity progressively increasing with increasing interfacial density.[4] Similar strategies have been employed more recently in the case of oxides, with varying degrees of success. For example, Kosacki and co-workers reported that the oxygen ion conductivity of Y_2O_3-stabilized ZrO_2 (YSZ) is significantly

enhanced when grown on MgO substrates.[10] Other studies of this system have not found the same enhancement.[11,12] Korte *et al.* found ionic conductivity to increase linearly with increasing density of phase boundaries in YSZ/Y_2O_3 heterostructures, and the activation energy was found to decrease for strained YSZ layers.[13] There has been much debate on enhanced ionic conductivity along YSZ/$SrTiO_3$ heterointerfaces. Garcia-Barriocanal *et al.* reported an eight order-of-magnitude increase in oxygen ion conductivity,[14] although others have argued that the enhanced conduction in that system is electronic rather than ionic in origin.[15] These studies not only illustrate the potential of heterointerfaces in modulating ionic transport, but also the difficulty in understanding the conduction behavior of oxide interfaces, advancing arguments on the effects of space charge, epitaxial strain and composition variations on ionic conductivity in multilayers. From a computational perspective, there have been several recent first-principles studies aimed at improving the understanding of the properties of polar interfaces.[16–21] Electronic and ionic redistribution were shown to lead to compensation of extra charge at the interface resulting in considerable changes in electronic structure of oxide heterostructures.

The perovskite $LaGaO_3$ (LGO) is an insulator, with very low ionic conductivity. Both La and Ga retain their valence state (+3) in oxides, so when LGO is doped with lower valence cations such as Sr and/or Mg, the oxygen vacancy concentration can be substantially increased. Doped LGO exhibits oxygen ion conductivity comparable to the best oxygen ion conductors.[22] Creating negatively charged interfaces with another material is another possible route to increasing the oxygen vacancy concentration in LGO and possibly inducing enhanced ionic conductivity in the space charge layers adjacent to the interfaces. Here we demonstrate that heterointerfaces in LGO heterostructures with spinel-structured $MgAl_2O_4$ (MAO) can be designed to create negatively charged interfaces. MAO is an insulator with a wide band gap and single-valence cations (+2 and +3 for Mg and Al, respectively). Thus, a charged interface between MAO and perovskite LGO is unlikely to be compensated electronically. A good epitaxial match between MAO and LGO and similar thermal expansion coefficients also motivate our choice of these two materials for this study.

Our strategy to induce higher vacancy concentrations involves the use of charged atomic planes as building blocks, as charged surfaces and interfaces require compensation to maintain overall electrical neutrality. Uncompensated polarity in semi-infinite systems causes diverging electric fields, and much work has been devoted to these issues.[23] The compensa-

tion is typically achieved by redistribution of electronic charges, changes in local composition at the interface or screening by mobile ions in the space-charge layer. In the presence of mobile charge carriers near an interface, a space charge layer arises, which can be described by the Poisson-Boltzmann equation, assuming purely electrostatic interactions with the interface and each other. However, the specific interactions of mobile carriers with interfacial species near the interface can modify the expected behavior due to variations in the composition, bonding, and structure at the interface in comparison to the bulk. We explore how these interactions can be investigated using first-principles methods and whether they can be included in continuum models.

In this work, we investigate an interface between the perovskite LGO, and the spinel MAO, which both exhibit alternating positive and negative charged (001) planes. Experimentally, perovskite-spinel heterointerfaces are known to form spontaneously as a result of phase separation.[24] The interfacial planes of both materials in our model are negatively charged, giving rise to an excess negative charge that is compensated by oxygen vacancies in the space charge layer. Thus, the heterostructure maintains overall electrical neutrality and, at the same time, allows us to investigate different vacancy distributions next to the interface and determine specific interactions. We compare electronic and ionic compensation mechanisms and determine electron density distributions self-consistently in each case via first-principles calculations. Based on the results of those calculations, we model band-bending and distributions of vacancies using the Poisson-Boltzmann equation. The rest of the paper is organized as follows. In Section II, the computational methods and parameters are provided. In Section III, we present results for the computed properties of bulk LGO and MAO phases with and without vacancies, followed by structural energetics and electronic structures of the LGO(001)//MAO(001) interfaces for different oxygen vacancy distributions. In Section IV, our results from first principles computations are used to estimate the distribution of charged vacancies within the framework of the Poisson-Boltzmann equation. Finally, we summarize our results in Section V.

II. COMPUTATIONAL DETAILS

A. Method

All calculations were performed within the framework of density functional theory (DFT) using the projector augmented wave method as implemented in VASP with the Perdew-Burke-Ernzerhof exchange-correlation functional.[25] Unless specified otherwise in the next subsection, we used a cutoff energy of 530 eV for wavefunctions. The **k**-point meshes for structure optimizations, total energy, and density-of-states (DOS) calculations for the various structures considered are also given in the next subsection. All structures were optimized using criteria of total-energy-convergence to within 0.1 meV and residual forces to less than 0.02 eV/Å. DOS calculations were performed using the tetrahedron method. For DOS and total energy calculations of the relaxed structures, the number of **k**-points and the energy cutoff for wavefunctions were chosen in order to ensure energy convergence to within 0.01 eV. Bader analysis was used to determine ionic charges.

B. Computational Procedures

1. Bulk

First, we optimized geometries of bulk LGO and MAO structures. Of the three polymorphs for LGO (cubic, orthorhombic and rhombohedral), we performed calculations using the orthorhombic structure (o-LGO), which is known to be the one with the lowest ground state energy.[30] Full structural optimization for o-LGO was performed on a supercell containing 20 atoms, starting from the experimental lattice constants[26] $a = 5.523$ Å, $b = 5.491$ Å, and $c = 7.772$ Å, using a $4 \times 4 \times 4$ **k**-point mesh. For MAO bulk calculations, a cubic supercell containing a total of 56 atoms was considered. Starting from the experimental cubic lattice parameter[27] $a = 8.075$ Å, the structure was fully optimized using a $6 \times 6 \times 6$ **k**-point mesh.

For structural optimization of LGO or MAO structures with oxygen vacancies (V_O) we used supercell models. For LGO we used a $\sqrt{2} \times \sqrt{2} \times 1$ supercell and considered three different cases: one V_O per cell (since the structure is quasi-cubic, various oxygen sites can be considered to be equivalent), two V_O's located at the maximal separation in the

same LaO plane, and two V_O's located at the maximal separation in the same GaO_2 plane. The in-plane distance between two V_O sites is $\sqrt{2}a = 5.77$ Å. Geometry optimization for one V_O in MAO was done using the same supercell as in the bulk calculations. In these geometry optimizations, only the internal parameters were allowed to relax, keeping the lattice parameters fixed at their previously optimized values. In vacancy calculations we used $3 \times 3 \times 3$ and $5 \times 5 \times 5$ **k**-point meshes, and wavefunction energy cutoffs of 425 and 400 eV for LGO and MAO, respectively. DOS and single-point total energy calculations were performed using a $4 \times 4 \times 4$ **k**-point mesh for LGO bulk and a $10 \times 10 \times 10$ **k**-point mesh for MAO bulk. In cases of LGO and MAO with oxygen vacancies, DOS calculations were performed using $6 \times 6 \times 6$ and $10 \times 10 \times 10$ **k**-point meshes, respectively.

2. Heterostructure

The model of the LGO(001)//MAO(001) interface was constructed by putting together a GaO_2-terminated LGO slab and an AlO_2-terminated MAO slab. In this way LGO and MAO slabs have non-stoichiometric structures of the type $(GaO_2)^{1-}$/ $(LaO)^{1+}$/.../$(LaO)^{1+}$/$(GaO_2)^{1-}$, and $(AlO)^{1-}$/$(1/2Mg)^{1+}$/... /$(1/2Mg)^{1+}$/$(AlO)^{1-}$, respectively, where charge per plane is given under the assumption that the ions are in their formal valence states. Since formation energies are significantly higher in the MAO structure, the extra charge due to deviations from stoichiometry is compensated by oxygen vacancies in the LGO part of the structure. The MAO portion of the (001) superlattice used in our calculations consists of 5 $(AlO)^{1-}$ and 4 $(1/2Mg)^{1+}$ stacking planes, amounting to a total of 64 atoms. For the LGO part, we used 9 $(GaO_2)^{1-}$ and 8$(LaO)^{1+}$ intermediate planes, in order to minimize the interaction between the periodic negatively charged interfaces and also to ensure a more "bulk-like" behavior away from the boundary. As a result the present model for the LGO//MAO heterostructure has the form: $(GaO_2)^{1-}\{(LaO)^{1+}(GaO_2)^{1-})\}_8//(AlO)^{1-}\{(1/2Mg)^{1+}(AlO)^{1-}\}_5$, with a total of 232 atoms. The LGO(001)//MAO(001) interface is shown schematically in Fig. 1.

In the present work, MAO is considered to be a substrate with multilayers of LGO and MAO grown on top of it. Therefore, the lattice parameters of quasi-cubic LGO along x and y directions (considering z to be the direction perpendicular to the interface) were fixed at the optimized lattice parameter of (001) MAO to simulate epitaxy. All internal parameters were optimized, as well as the lattice parameter along z for the whole supercell. Among

the various configurations for the heterostructure of LGO on MAO, we have chosen the one with the lowest total energy, and used it in order to construct the initial structures of the interfacial structures with different vacancy configurations considered. Oxygen vacancies in the heterostructure were created in LaO and GaO_2 planes located at different distances from the interface with the same in-plane separations between two V_O sites as in the bulk.

C. Chemical Potentials

The formation energy for oxygen vacancies (E_{V_O}) per vacancy was calculated using

$$E_{V_O} = \frac{E_t(V_O) - E_t}{N_{V_O}} + \mu_O, \tag{1}$$

where $E_t(V_O)$ and E_t refer to the total energies of the systems with and without V_O, respectively, and N_{V_O} is the number of vacancies. The system is assumed to be in equilibrium with O_2 in gas phase. Therefore, the chemical potential of oxygen at temperature T and partial pressure p is uniquely determined as $\mu_O = \frac{1}{2}\mu_{O_2(\mathrm{gas})}(T,p)$, which can be expressed in terms of the chemical potential of oxygen at temperature T and $p^0 = 1$ atm partial pressure as $\mu_{O_2(\mathrm{gas})}(T,p) = \left(\mu_{O_2}(T,p^0) + kT\ln\frac{p}{p^0}\right)$. The expression for $\mu_{O_2}(T,p^0)$ can be obtained by dividing it into enthalpy (H) and entropy (S) contributions as

$$\mu_{O_2}(T,p^0) = \left(H_{O_2}(T,p^0) - H_{O_2}(0,p^0)\right) - TS_{O_2}(T,p^0) + H_{O_2}(0,p^0). \tag{2}$$

Assuming that $H_{O_2}(0,p^0)$ corresponds to the total energy of the O_2 molecule, and by obtaining H and S from thermochemical tables,[31] the above equations can be combined to give μ_O at any given T and p. In order to compute the total energy of O_2 in the gas phase, we placed an O_2 molecule in a $14 \times 15 \times 16$ Å^3 supercell, and performed spin-polarized calculations with an energy cutoff of 900 eV for the wavefunctions and Γ-point sampling.

The interface energy for a LGO//MAO heterostructure is defined as

$$E_{\mathrm{int}} = (E_t - N_{\mathrm{La}}\mu_{\mathrm{La}} - N_{\mathrm{Ga}}\mu_{\mathrm{Ga}} - N_{\mathrm{Mg}}\mu_{\mathrm{Mg}} - N_{\mathrm{Al}}\mu_{\mathrm{Al}} - N_{\mathrm{O}}\mu_{\mathrm{O}})/2A, \tag{3}$$

where E_t is the total energy of the LGO//MAO system, A is an interface area per supercell and N_X, μ_X refer to the number of atoms of type X in the supercell and their chemical potentials in respective bulk oxides. The factor of 2 accounts for the fact that by construction there are two identical interfaces in a periodic LGO//MAO supercell. In order to evaluate

the limits on chemical potentials of Ga and Al, calculations were also performed by full relaxations from the experimental parameters[28,29] of monoclinic $\beta - Ga_2O_3$ and trigonal $\alpha - Al_2O_3$ using **k**-point meshes of $4 \times 12 \times 8$ and $6 \times 6 \times 6$, respectively.

The chemical potentials are derived assuming thermodynamic equilibrium with $LaGaO_3$, $MgAl_2O_4$, Ga_2O_3 and Al_2O_3, which results in the following set of equations:

$$\mu_{La} + \mu_{Ga} + 3\mu_O = \mu_{LaGaO_3}, \tag{4}$$

$$\mu_{Mg} + 2\mu_{Al} + 4\mu_O = \mu_{MgAl_2O_4}, \tag{5}$$

$$2\mu_{Ga} + 3\mu_O = \mu_{Ga_2O_3}, \tag{6}$$

$$2\mu_{Al} + 3\mu_O = \mu_{Al_2O_3}, \tag{7}$$

where μ_{LaGaO_3}, $\mu_{MgAl_2O_4}$, $\mu_{Ga_2O_3}$, and $\mu_{Al_2O_3}$ are the calculated total energies per formula unit of bulk LGO, MAO, Ga_2O_3, and Al_2O_3, respectively. We calculate vacancy formation energy (Eq. 1), and interface energy E_{int} (Eq. 3) by expressing all of the individual cation chemical potentials from Eqs. 4-7 along with Eq. 2 for μ_O .

III. RESULTS AND DISCUSSION

A. Calculated Structures and Electronic Properties of Bulk LGO and MAO

The optimized bulk lattice parameters along with corresponding experimental values for LGO and MAO are given in Table I. For both LGO and MAO, the calculated lattice parameters are slightly overestimated, by $\approx 1\%$, with respect to the corresponding experimental values, giving a lattice mismatch of 4.2%, slightly bigger than the experimental value of 3.7%.

Figure 2 shows the computed partial DOS for bulk LGO and MAO. The calculated bandgap values are given in Table I. As expected, LGO shows an insulating behavior with a bandgap of 3.74 eV, which is underestimated with respect to the experimental value of 4.4 eV, but in agreement with previous DFT calculations using GGA.[32] The main contributions to the DOS at the top of the valence band are from the hybridized O $2p$, and Ga $3d$ and $4p$ states. In the conduction band, the high intensity peak at ≈ 5 eV represents the unoccupied La $4f$ states. For MAO, a bandgap of 5.00 eV is underestimated with respect to the experimental value of 7.8 eV.[33] The upper valence band contains mostly O $2p$ orbitals,

while the lower part of the conduction band corresponds to unoccupied Al $3p$ and Mg $3s$ orbitals. These results for MAO are also in good agreement with previous DFT calculations using GGA.[34]

B. Oxygen vacancies in bulk LGO and MAO

We performed geometry optimization of structures with oxygen vacancies created in the LGO and MAO bulk as described in the previous Section. The formation energies for $V_{\rm O}$ in LGO and MAO were calculated using different concentrations of vacancies, $N_{V_{\rm O}}/N_{\rm O}$, where $N_{V_{\rm O}}$ and $N_{\rm O}$ are the number of $V_{\rm O}$'s and available O sites in the supercells, respectively. We considered $N_{V_{\rm O}}/N_{\rm O}$ values of 1/32 for MAO and 1/24 and 2/24 for LGO. The results for the formation energies $E_{V_{\rm O}}$ (Eq. 1) are given in Table II. They show that the vacancy formation energy for MAO at the lowest calculated concentration is significantly higher than that for LGO (by ≈ 1.5 eV), suggesting that in an LGO//MAO heterostructure the formation of $V_{\rm O}$ should be energetically more favorable in the LGO subsystem than in MAO.

Next, we consider interactions between vacancies in LGO by comparing calculations with different oxygen vacancy concentrations. Table II shows formation energy of oxygen vacancy for 1/24 and 2/24 vacancy concentrations, respectively. In the latter case, two $V_{\rm O}$'s, instead of one, are created in bulk LGO. In this case two scenarios were considered: two $V_{\rm O}$'s located in (a) a GaO_2 plane and (b) a LaO plane. The $V_{\rm O} - V_{\rm O}$ distance of 5.77 Å, was the same in both cases, which is the maximum possible in-plane distance for $V_{\rm O}$'s in the present supercell configuration. As indicated by the formation energies in Table II, the interaction of vacancies is repulsive and relatively weak, with interaction energies of 0.025 and 0.07 eV per vacancy for $V_{\rm O}$'s in GaO_2 and LaO planes, respectively, resulting in similar vacancy formation energies for 1/24 and 2/24 concentrations. Comparing the formation energies of vacancies in LaO versus the GaO_2 planes at the same concentrations, we find the vacancies to have a slight preference to be in a GaO_2 plane (by 0.045 eV). We note that in the bulk structures vacancies are formally not charged, since a neutral O atom is removed from the supercell to create a vacancy. In the forthcoming discussion of results for the heterostructures, each heterostructure considered in our calculations formally has a total of $-4e$ extra charge at the interface (per supercell), which requires two compensating positively charged oxygen vacancies, denoted by $V_{\rm O}^{\bullet\bullet}$ in the Kröger-Vink notation. Therefore, vacancy

interactions in the bulk LGO and in the heterostructure might not be directly comparable.

C. Structure and Interface Energies of the LGO//MAO Heterostructures

In our model of the LGO//MAO interface, a GaO_2 plane of LGO with a nominal charge of $-1e$ per formula unit is placed next to an AlO_2 plane of MAO with the same nominal charge of $-1e$ per formula unit, introducing an extra negative charge at the interface. In polar interfaces, the required charge compensation may be achieved by different mechanisms,[17,18,23] such as (i) a change in the number of electrons, as in $AlO_2/LaO/TiO_2$ interfaces in $LaAlO_3//SrTiO_3$ superlattices, where the extra electrons are placed in the $SrTiO_3$ conduction band, and/or (ii) by an atomic reconstruction, as in the case of the $AlO_2/SrO/TiO_2$ interfaces,[16] where charge compensation is achieved by the introduction of oxygen vacancies.[35] In order to compare different compensation mechanisms and to find the most favorable, we considered the following configurations: (a) LGO//MAO interface with no vacancies, (b) LGO//MAO interface fully compensated by oxygen vacancies.

As mentioned above, for the heterostructure model considered here, two V_O's (per each of two interfaces in the supercell) are required to achieve compensation, since each GaO_2 or AlO_2 plane is represented by a total of four formula units in the supercell, resulting in an extra charge of $-4e$ per interface. In order to compare different vacancy arrangements in the heterostructure in the latter case, we calculated the LGO//MAO heterostructure with two vacancies per interface located in either the GaO_2 or LaO plane at different distances from the interface. The two V_O's were created in either GaO_2 or LaO planes by removing negatively charged oxygen ions, thus making overall heterostructure electrically neutral (i.e. compensated).

Optimized geometries of heterostructures with vacancies in either of the first three layers are shown in Fig. 3. For a more quantitative description of the structures, average displacements along z for atoms located in planes 1, 2 and 3 of LGO are presented in Fig. 4. When the vacancies are in the first layer, the oxygens in this layer displace outward by about 0.3 Å on average, driven by electrostatic interactions with a negatively charged interface. Displacements of cations in the first three layers are small in this structure. There is a nearly uniform out-of-plane compressive strain beyond the third layer, which is a common feature of all three structures presented in Fig. 3. Structures corresponding to vacancies in the sec-

ond (GaO_2) and third (LaO) planes are characterized by a more pronounced reconstruction in the interface region. When the vacancies are in the second plane (LaO), two of the Ga ions in the GaO_2 plane adjacent to the interface move towards the MAO region by about 0.15 Å following the pattern of Mg ions. The outward displacement of O atoms by 0.4 Å on average is somewhat higher than in the previous case. When the vacancies are in the third plane (GaO_2), the two Ga ions align with Mg ions and are located exactly where the next layer of Mg atoms would be located in a periodic MAO structure. The displacements of O atoms, on the other hand, are much smaller than in previous cases. We note that the crystal field effects are expected to be strong in MAO because of the predominantly ionic character of bonding. This favors location of positive atoms (Ga) in LGO near the interface in ionic positions (Mg) of the truncated MAO lattice. Additional explanation for this structural rearrangement is a higher structural flexibility of the interfacial planes as a result of removing oxygens from the second or third planes, which weakens the bonding between the first planes next to the interface. This results in more degrees of freedom for interface reconstruction. This is not the case when vacancies are removed either from the first plane or from planes beyond the third plane into the LGO structure (not shown).

The formation energies of oxygen vacancies were calculated using Eq. (1). Here, all energies are referenced to the same heterostructure without vacancies referred to in the compensation mechanism (a) above. These relative energies of formation are plotted in Fig. 5. In many cases, due to the underestimation of bandgaps, the application of LDA or GGA exchange functionals results in incorrect formation energies. The effects are stronger when charged defects are introduced into the system, but also occur when neutral defects introduce new single-particle states that are occupied by electrons. This does not apply to our case (LGO//MAO), where neutral oxygen atoms are removed from the system and where, apart from a small reduction in the bandgap, no new single-particle states were observed in the DOS.[36] Negative vacancy formation energy indicates that an oxygen vacancy would be preferred to electronic charge transfer in order to compensate the excess charge at the interface. This is the case for vacancies belonging to planes 1 (GaO_2), 2 (LaO), and 3 (GaO_2), but not for vacancies located deeper in bulk LGO. The minimum in energy is achieved when the vacancies are located in plane 3 (GaO_2), corresponding to the most stable configuration. We can also calculate the formation energies for V_O's in different planes as a function of the oxygen partial pressure in the range from 10^{-12} to 1 atm at room temperature

(using the formalism summarized in Section II.C). The results for the first five planes are shown in Fig. 6.

Interface energies for the heterostructure with V_O's in the third (GaO_2) plane and for the heterostructure without vacancies were calculated using Eq. (3). Typical values for interface energies are $\approx 1 - 3$ J/m^2. The results for the interface energies for the two cases - without vacancies and with vacancies in the third plane - are shown as a function of the oxygen partial pressure in Fig. 7. We observe that even for very high pressures the interface with vacancies has the lower energy.

D. Charge distribution and electronic properties of LGO//MAO heterostructures

Since the electron distributions in our calculations are determined self-consistently, the electrons in the nominally charged planes can redistribute. For example, if one-electron levels associated with vacancies are lower in energy than the states in the interfacial planes, the vacancies might trap electrons and change their valence state. This is likely to affect charge compensation mechanisms and ionic conductivity in the space charge layer. In order to investigate charge compensation in the LGO//MAO heterostructure in detail, we address electron charge distribution. A Bader analysis was performed to obtain the charge state for each atom in the heterostructure and then these values were summed up for each atomic plane parallel to the interface in order to calculate the total charge per plane.

The charge profile for the structure with V_O's created in the third (GaO_2) planes from each interface is shown in Fig. 8. As expected, the MAO is more ionic than LGO. In fact, the charges per plane for MAO are twice higher than those for LGO despite the fact that the nominal charges of the planes obtained by summing up formal charges of the constituent ions are the same in both materials. The charges in the planes away from the interface are very similar to bulk charges, with the notable exception of the planes with V_O's. It is evident that after vacancy creation and relaxation the interface remains negatively charged, while V_O's exhibit positive charge and do not accept electrons from the interfacial planes or elsewhere. This charge state corresponds to two $V_O^{\bullet\bullet}$ located in the third (GaO_2) plane.

Next we consider the effect of different compensation mechanisms on the electronic structure. Since it is known that DFT produces bandgaps that are too low compared to experimental values, these results should be taken as qualitative. The bandgaps for heterostruc-

tures with different positions of the plane in which the vacancies are located are plotted in Fig. 9. As the vacancies are placed farther away from the interface, the bandgaps decrease. However, for the configuration with the lowest energy in our calculations (vacancies in the third plane), the heterostructure is still insulating and exhibits a bandgap of 1.78 eV. The bandgaps become small for heterostructures with vacancies located beyond the fourth plane. This decrease in the bandgap with the increasing distance between the plane containing the vacancies and the interface, can be qualitatively understood as sketched in Fig. 9. The negative charge at the interface plane together with the positive charge of the plane containing the vacancies creates an electric field inside the LGO region in-between these two planes, thus generating a linear potential that bends both the valence and conduction bands. The bandgap, calculated as the difference between valence band maximum and conduction band minimum, decreases linearly with the distance. If we use an extrapolation, a large concentration of vacancies away from the interface would result in a metallic state as the distance increases. This is in contrast to the compensation mechanism without the vacancies, where the position of compensating charge does not vary. Therefore, predominantly ionic conductivity seems to be possible, since the heterostructure maintains the band gap with the compensating vacancies at the most favorable distance from the interface. In the next section, we consider the distribution of vacancies in order to validate this point.

IV. VACANCY DISTRIBUTION USING THE POISSON-BOLTZMANN EQUATION

In the previous sections we have determined the formation energies, charge states and microscopic configurations for vacancies in the LGO//MAO heterostructure at 0 K within the framework of DFT. However, it is also important to know how vacancies would be distributed at finite temperatures and thus to determine the spatial extent of the charge-compensating layer. One way to give a macroscopic description of the LGO//MAO system at finite temperature is to consider the Poisson-Boltzmann (P-B) equation, which has been used by others in the study of carrier distribution in ionic conductors.[38,39] Within this approach, the distribution of charged carriers in the presence a surface charge density is determined by their electrostatic energy and the Boltzmann statistics. The input parameters for this model are the dielectric constant of the medium, the charge density at the interface and the

charge of each mobile particle [in this case, oxygen vacancies ($V_O^{\bullet\bullet}$)]. First, we establish a correspondence between the input parameters of the P-B model and our DFT results. We start by noticing that the formation energy for $V_O^{\bullet\bullet}$'s displayed in Fig. 5 can be thought as composed of two contributions: on the one hand the energy resulting from the electrostatic interaction between the charged vacancy (charge $+2e$) and the negatively charged interface (E_e), and on the other hand an intrinsic contribution (E_i) which includes short-range effects (such as structural, chemical, etc.). In this way we can write $E_{V_\mathrm{O}} = E_i + E_e$. Guided by the discussion in the previous section (Fig. 9c), we can express the electrostatic contribution as

$$E_e = \frac{\sigma e}{\epsilon_r \epsilon_0} z, \tag{8}$$

where z is the coordinate in the direction perpendicular to the interface, σ is the charge density at the interface, and ϵ_r is the relative dielectric constant of LGO. From Fig. 5, we observe that the formation energy per $V_O^{\bullet\bullet}$ grows almost linearly starting from plane 3 (GaO_2 layer) and going into the bulk. We conclude from this observation that when the vacancies are located closer to the interface than the third atomic plane, the electrostatic contribution to E_{V_O} is not the dominant contribution to the vacancy energy since strong structural rearrangement in the interfacial region results in E_{V_O} approximately equal to E_i. On the other hand, if the vacancies are located farther away from the interface than the third plane, the relaxations in the first several planes next to the interface are much smaller and the electrostatic energy of these vacancies can be reasonably approximated by Eq. 8. Thus, by assuming that the intrinsic contribution to the vacancy formation energy, E_i, is a constant, we can calculate σ/ϵ_r from the slope of the interpolating line shown in Fig. 5. Taking into account that σ is determined by the extra charge placed at the interface, and using the value that corresponds to $-4e$ per unit cell ($\sigma = -0.96$ C/m^2), we obtain $\epsilon_r = 24.8$, which is in very good agreement with the experimental value of 25.20 at room temperature for the (001) direction.[37] Such a good agreement between the microscopic (DFT) and the macroscopic (electrostatic) models, serves as a validation for the applicability of the P-B analysis developed in the rest of this section. We can now write the P-B equation for $V_O^{\bullet\bullet}$'s (charge $+2e$) in the LGO part of the heterostructure as

$$\frac{d^2\phi}{dz} = -\frac{2e\rho_0}{\epsilon_r \epsilon_0} e^{-\frac{2e\phi}{k_B T}}, \tag{9}$$

where ρ_0 is defined as the density of vacancies at a point where the potential $\phi(z)$=0, and can be determined by the requirement that the charge at the interface is compensated by the total charge of the vacancies. This equation takes into account the fact that the potential due to the interfacial charge density is screened by the vacancies. Solving Eq. 9, we obtain the density of vacancies as a function of z

$$\rho(z) = \frac{\epsilon_r \epsilon_0 k_B T}{2e^2 \left(z + \frac{\epsilon_r \epsilon_0 k_B T}{e\sigma}\right)^2}. \tag{10}$$

In Fig. 10 we plot the vacancy concentration as a function of the distance to the interface for temperatures of 300 and 800 K, respectively. In order to show how the value of the interfacial charge would affect the equilibrium distribution, we also plot the concentration of vacancies for different interfacial charge densities (σ/10 and σ/100). We observe that for $\sigma = -0.96$ C/m^2 at both temperatures the density of vacancies decreases abruptly when going away from the interface, which means that most vacancies are located in plane 3. For an interfacial charge density of σ/100, vacancies would distribute more uniformly across the structure.

It is illustratrive to compare resulting distributions with the highest vacancy concentration ($\approx 10^{21}$cm^{-3}) of Sr- and Mg-doped LGO.[40] In the LGO//MAO heterostructure (where $\sigma = -0.96$ C/m^2) the concentration of vacancies at a distance of 4 Å from the interface (plane 3) is more than two orders of magnitude higher than for the Sr- and Mg-doped case, either at 300 or 800 K. Since the value of σ is relatively large, the concentration of vacancies in Eq. (10) decreases like $1/z^2$ (z is measured from plane 3) when going away from the interface into LGO bulk. Therefore, at 800 K the density of vacancies 6 Å away from the interface (plane 4) is of the same order of magnitude as in the doped bulk. For that reason, to design a nanostructure with minimal vacancy concentration similar to that of Sr- and Mg-doped bulk LGO, the total thickness of the LGO slab should be below twice 6 Å. It is likely that high ionic conductivity in the LGO//MAO system could be achieved at lower average vacancy concentrations than in the doped LGO, due to decreased interactions between the charged carriers and the dopants,[6] resulting in higher mobility in the heterostructure.

From the P-B model we can also obtain the difference of potential between the interface and a point at a distance z from it in LGO as

$$\phi(z) - \phi(0) = \frac{k_B T}{e} ln \left[1 + \frac{e\sigma z}{\epsilon_r \epsilon_0 k_B T} \right]. \quad (11)$$

Earlier we have mentioned that one of the requirements for a good ionic conductor was the absence of any electrical conductivity. We have shown that at $T = 0$ K the LGO//MAO heterostructure remained insulating for all the different vacancy configurations (Section III.D). Now we can revisit this question in the light of the P-B formalism. In order to have electronic conductivity in the system the electrostatic energy of an electron should be enough to promote this electron from the valence to the conduction band, overcoming the bandgap. For that to happen $E_{\text{gap}} = e\,[\phi(z) - \phi(0)]$, where E_{gap} corresponds to the bandgap for bulk LGO calculated to be 3.74 eV (more than 1 eV smaller than the bandgap for MAO). Using this condition together with Eq. (11) and solving for z, it is possible to estimate the value of the critical thickness of the LGO part of the heterostructure for which electronic conductivity will start to occur. In this case, the values we obtain for the critical thickness are well above the possible heterostructure size, even for a temperature of 1000 K, indicating that electronic conductivity would be very unlikely in the system. Therefore, according to this model, even for high temperatures our LGO//MAO heterostructure would remain insulating.

V. SUMMARY

We have studied the possibility of enhancing ionic conductivity in LGO by the design of LGO//MAO heterostructures with excess negative charge in the interfacial planes. Our study reveals that compensation by oxygen vacancies is a favorable mechanism for thin LGO slabs. DFT calculations for vacancies placed at different distances from the interface exhibit a non-monotonic formation energy behavior in the first three planes, followed by a nearly linear increase in energy consistent with electrostatic interactions. The vacancy formation energy was found to be the lowest for vacancies located in the third LGO plane away from the interface. Calculated charge distributions indicate that there is no charge migration/redistribution from the negatively charged interface towards the bulk, and that the compensating vacancies exhibit a charge consistent with a charge state $V_{\text{O}}^{\bullet\bullet}$. Furthermore, we showed that although there is a decrease in the bandgap, the LGO//MAO heterostructure with vacancies still remains insulating. These two conditions, i.e. the presence of charged

ionic defects and the absence of electronic conductivity, are essential requirements for a good ionic conductor. Finally, based on these results, a Poisson-Boltzmann model was used in order to describe the vacancy distribution, showing that even at high temperatures most vacancies are highly localized around the first atomic planes of the LGO structure and that electronic conduction is very unlikely. In light of the recent advances in synthesis of oxide heterostructures and the encouraging first-principles results reported here, we therefore suggest that it is possible to synthesize such a heterostructure with excess negative charge at the interfaces. This is likely to lead to enhanced ionic conductivity in such a layered system.

ACKNOWLEDGMENTS

This work was supported by the U. S. Department of Energy, Office of Science, Office of Basic Energy Sciences under Contract No. DE-AC02-06CH11357. We acknowledge computational support from the Argonne National Laboratory Computing Resource Center, Center for Nanoscale Materials, and the National Energy Research Scientific Computing Center, which is supported by the Office of Science of the US Department of Energy.

---

* zapol@anl.gov

[1] R. A. De Souza, Phys. Chem. Chem. Phys., **11**, 9939 (2009).

[2] X. Guo and R. Waser, Prog. Mater. Sci., **51**, 151 (2006).

[3] J. Maier, Progress in Solid State Chemistry, **23**, 171 (1995).

[4] N. Sata, K. Eberman, K. Eberl, and J. Maier, Nature **408**, 946 (2000).

[5] E. D. Wachsman and K. Taek Lee, Science **334**, 935 (2011).

[6] M. S. Islam, Solid State Ionics, **154155**, 75 (2002).

[7] M. Sase, K. Yashiro, K. Sato, J. Mizusaki, T. Kawada, N. Sakai, K. Yamaji, T. Horita and H. Yokokawa, Solid State Ionics, 178, 18431852 (2008).

[8] M. Sase, F. Hermes, K. Yashiro, K. Sato, J. Mizusaki, T. Kawada, N. Sakai and H. Yokokawa, J. Electrochem. Soc., **155**, B793B797 (2008).

[9] K. Yashiro, T. Nakamura, M. Sase, F. Hermes, K. Sato, T. Kawada and J. Mizusaki, Electrochem. Solid-State Lett., **12**, B135B137 (2009).

[10] I. Kosacki, C. M. Rouleau, P. F. Becher, J. Bentley, and D. H. Lowndes, Solid State Ionics, **176**, 1319 (2005).

[11] X. Guo, S. Vasco, S. Mi, K. Szot, R. Wachsman, and R. Waser, Acta Mater., **53**, 5161 (2005).

[12] A. Karthikeyan, C.-L. Chang , and S. Ramanathan, Appl. Phys. Lett., **86**, 183116 (2006).

[13] C. Korte, A. Peters, J. Janek, D. Hesse and N. Zakharov, Phys. Chem. Chem. Phys., **10**, 4623, (2008).

[14] J. Garcia-Barriocanal , A. Rivera-Calzada , M. Varela , Z. Sefrioui , E. Iborra , C. Leon , S. J. Pennycook , J. Santamaria , Science , **321** , 676 (2008).

[15] X. Guo, Science, **324**, 465a (2009).

[16] R. Pentcheva and W. E. Pickett, Phys. Rev. B, **74**, 035112 (2006).

[17] R. Pentcheva and W. E. Pickett, Phys. Rev. Lett., **102**, 107602 (2009).

[18] R. Pentcheva and W. E. Pickett, J. Phys: Cond. Matt., **22**, 43001 (2010).

[19] V. K. Lazarov, M. Weinert, S. A. Chambers, and M. Gajdardziska-Josifovska, Phys. Rev. B, **72**, 195401 (2005).

[20] R. Oja and R. M. Nieminen, Phys. Rev. B, **80**, 205420 (2009).

[21] N. C. Bristowe, E. Artacho, and P. B. Littlewood, Phys. Rev. B **80**, 045425 (2009).

[22] T. Ishihara, H. Matsuda, Y. Takita, J. Am. Chem. Soc., **116**, 3801-3803 (1994).

[23] J. Goniakowski, F. Finocchi, and C. Noguera, Rep. Prog. Phys., **71**, 16501 (2008).

[24] H. Zheng, Q. Zhan, F. Zavalich, M. Sherburne, F. Straub, M. P. Cruz, L.-Q. Chen, U. Dahmen, R. Ramesh, Nano Lett., **6**, 1401 (2006).

[25] G. Kresse and J. Hafner, Phys. Rev. B **47**, 558 (1993); P. E. Blöchl, *ibid.* **50**, 17953 (1994).

[26] L. Vasylechko, A. Matkovski, A. Suchocki, D. Savytskii, and I. Syvorotka, J. of Alloys and Compds, **286**, 213 (1999).

[27] K. E. Sickafus and J. M. Wills, J. Am. Ceram. Soc., **82**, 3279 (1999).

[28] J. Ahman, G. Svensson, and J. Albersson, Acta Cryst., **C52**, 1336 (1996).

[29] http://www.mindat.org/min-1136.html

[30] A. Kuwabara and I. Tanaka, J. Phys. Chem. B **108**, 9168 (2004).

[31] NIST-JANAF Thermochemical Tables, http://kinetics.nist.gov/janaf/

[32] K. Ogisu, A. Ishikawa, Y. Shimodaira, T. Takata, H. Kobayashi, and K. Domen, J. Phys. Chem. C, **112**, 11978 (2008).

[33] M. L. Bortz, R. H. French, D. J. Jones, R. V. Kasowski, and F. S. Ohuchi, Phys. Scr.,**41**, 537 (1990).

[34] S. M. Hosseini, Phys. Stat. Sol. (b) **245**, 2800 (2008).

[35] N. Nakagawa, H. Y. Hwang, and D. A. Muller, Nat. Mat., **5**, 204 (2006).

[36] A. Janotti and C. G. Van de Walle, Phys. Rev. B **76**, 165202 (2007).

[37] D.C. Dube, H.J. Scheel, I. Reaney, M. Daglish, and N. Setter, J. Appl. Phys., **75**, 4126 (1994).

[38] J. Maier, Z. Phys. Chem. **219**, 35-46 (2005).

[39] E. Fabbri, D. Pergolesi, and E. Traversa, Sci. Technol. Adv. Mater. **11** 054503 (2010).

[40] P. Huang and A. Petric, J. Electrochem. Soc., **143**(5), 1644 (1996).

	Calculated				Experimental[26,27,32,33]			
		Lattice Parameters (Å)				Lattice Parameters (Å)		
	Bandgap (eV)	a	b	c	Bandgap (eV)	a	b	c
LGO	3.74	5.57	5.55	7.88	4.4	5.523	5.491	7.772
MAO	5.00	8.16	-	-	7.8	8.075	-	-

TABLE I. Calculated and experimental bandgaps and lattice parameters of LGO and MAO.

1/24 V_O concentration	**Formation Energy (eV)**
LGO	5.14
MAO	6.65
2/24 V_O concentration	
LaO plane (LGO)	5.28
GaO_2 plane (LGO)	5.19

TABLE II. Formation energies for V_O in bulk LGO and MAO. See the text for vacancy concentrations.

FIG. 1. Side view of initial configuration of the o-LGO//MAO interface. The interface is formed by $(AlO_2)^{-1}$ and $(GaO_2)^{-1}$ planes, which results in an excess negative charge. For o-LGO, tilted octahedra with a central Ga atom are displayed.

FIG. 2. Projected DOS for bulk LGO (top) and MAO (bottom). Both structures display insulating behavior with bandgaps calculated to be 3.74 and 5.00 eV, respectively.

FIG. 3. Relaxed structures of the LGO//MAO interface along (001) and (010) directions for vacancies located in (a) the first plane, (b) the second plane, and (c) the third plane. Small squares show the approximate location of the vacancies.

FIG. 4. Average displacements for La, Ga, O as a function of the plane in which they are located when V_O's are located in (a) the first plane, (b) the second plane, and (c) the third plane.

FIG. 5. Formation energies for oxygen vacancies located in different LGO planes. Starting at plane 3, formation energies can be linearly interpolated, as shown by a straight line, reflecting the effect of the electrostatic potential generated by the negative charge distribution at the interface. (See Section IV).

FIG. 6. Formation energies of oxygen vacancy calculated as a function of oxygen partial pressure (atm) at a temperature of 298.5 K. Each line corresponds to vacancies located in a different planes.

FIG. 7. Interface energy computed using Eq. (3) as a function of the oxygen partial pressure for an interface without any V_O's (solid line) and with V_O's located in the third (GaO_2) plane of LGO (dashed line).

FIG. 8. Total charge per plane for the LGO//MAO heterostructure with vacancies located in the third plane. (Blue) circles represent the location of the vacancies and dashed horizontal lines (green) represent the bulk values of the charge in the planes.

FIG. 9. (a) Bandgap as a function of the location of vacancies. (b) Schematic of the valence and conduction band bending in the region between the positively charged vacancies and the negatively charged interface. Indicated value of bandgap corresponds to the case when V_O's are located in the third plane. (c) Schematic of the electric field in LGO.

FIG. 10. Poisson-Boltzmann concentration of vacancies in LGO (log scale) calculated for different charge densities at the interface and at temperatures of (a) 300, and (b) 800 K. Dashed horizontal lines correspond to the highest concentration of vacancies in Sr- and Mg- doped LGO.

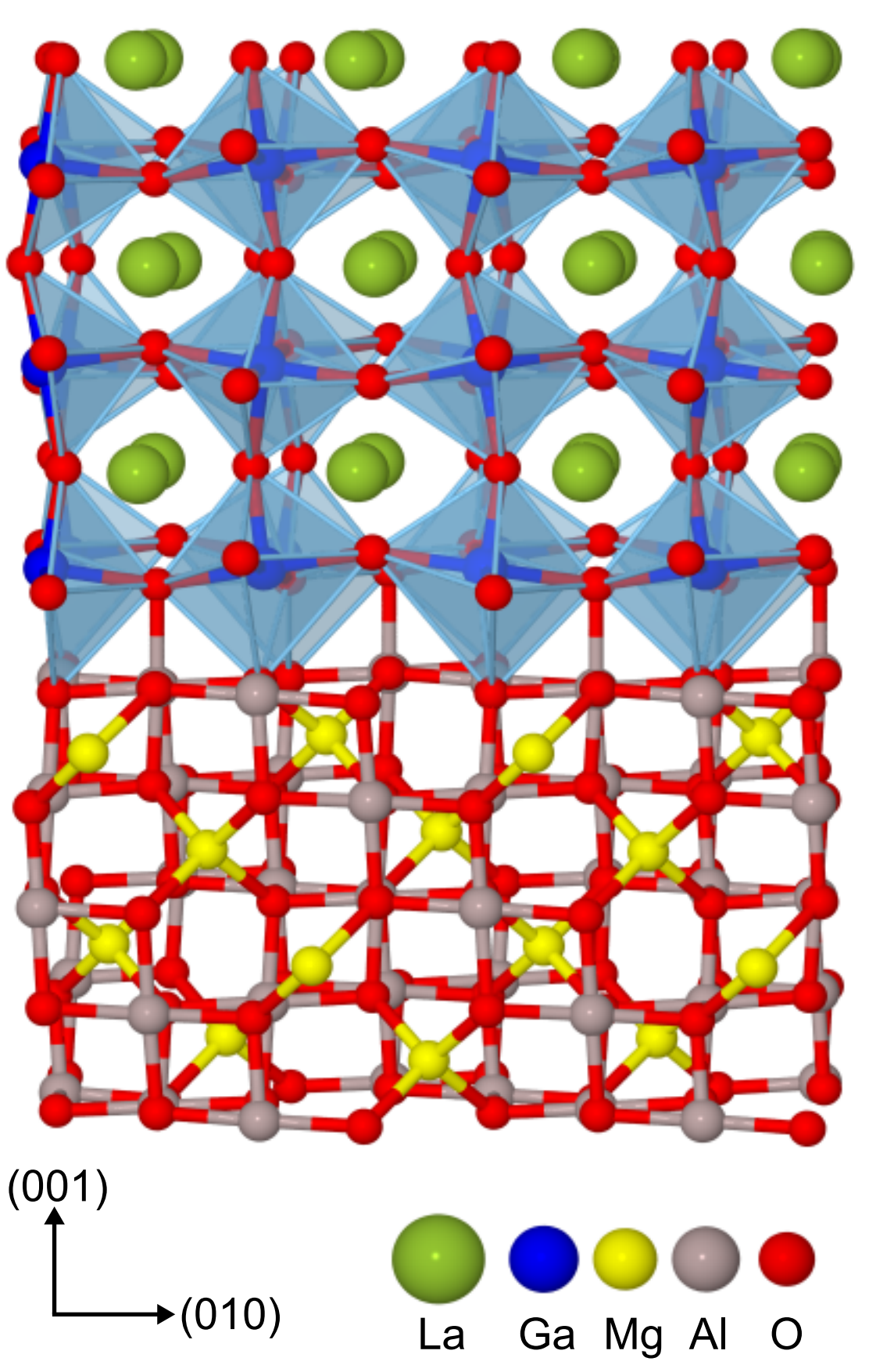
(001)
(010)
La
Ga
Mg
Al
O

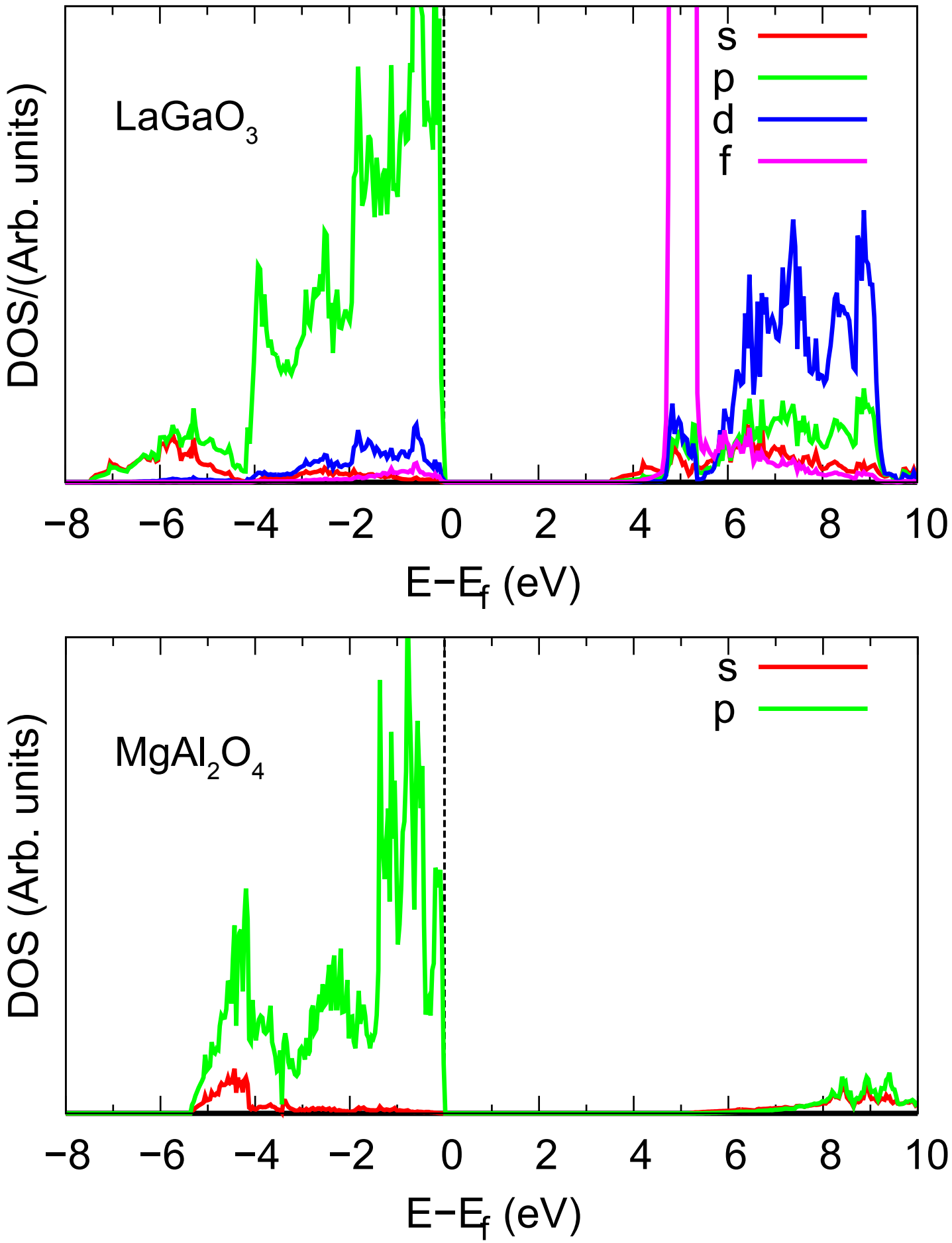
LaGaO3
s
p
d
f
DOS/(Arb. units)
−8
−6
−4
−2
0
2
4
6
8
10
E−Ef (eV)
MgAl2O4
s
p
DOS (Arb. units)
−8
−6
−4
−2
0
2
4
6
8
10
E−Ef (eV)

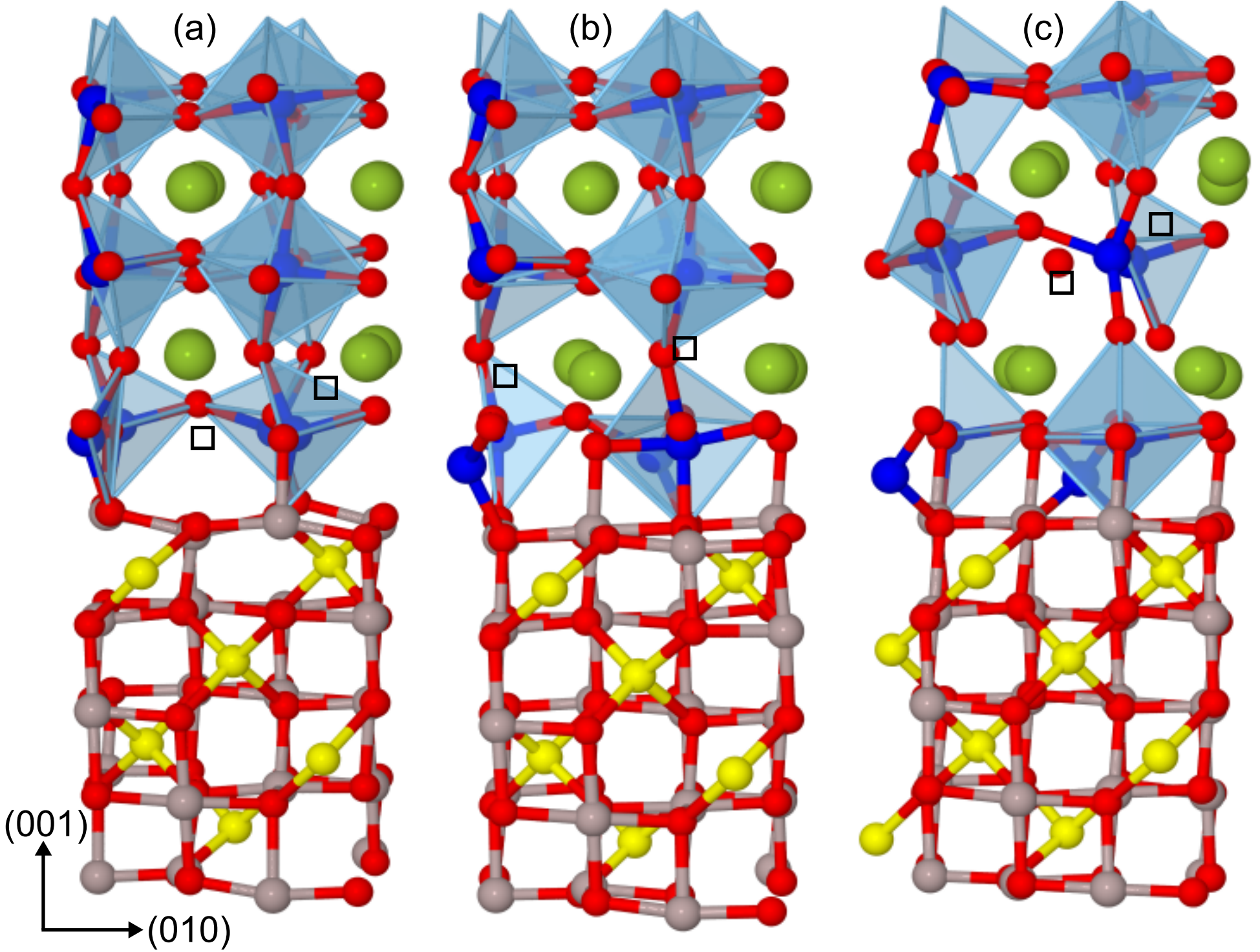
(a)
(b)
(c)
(001)
(010)

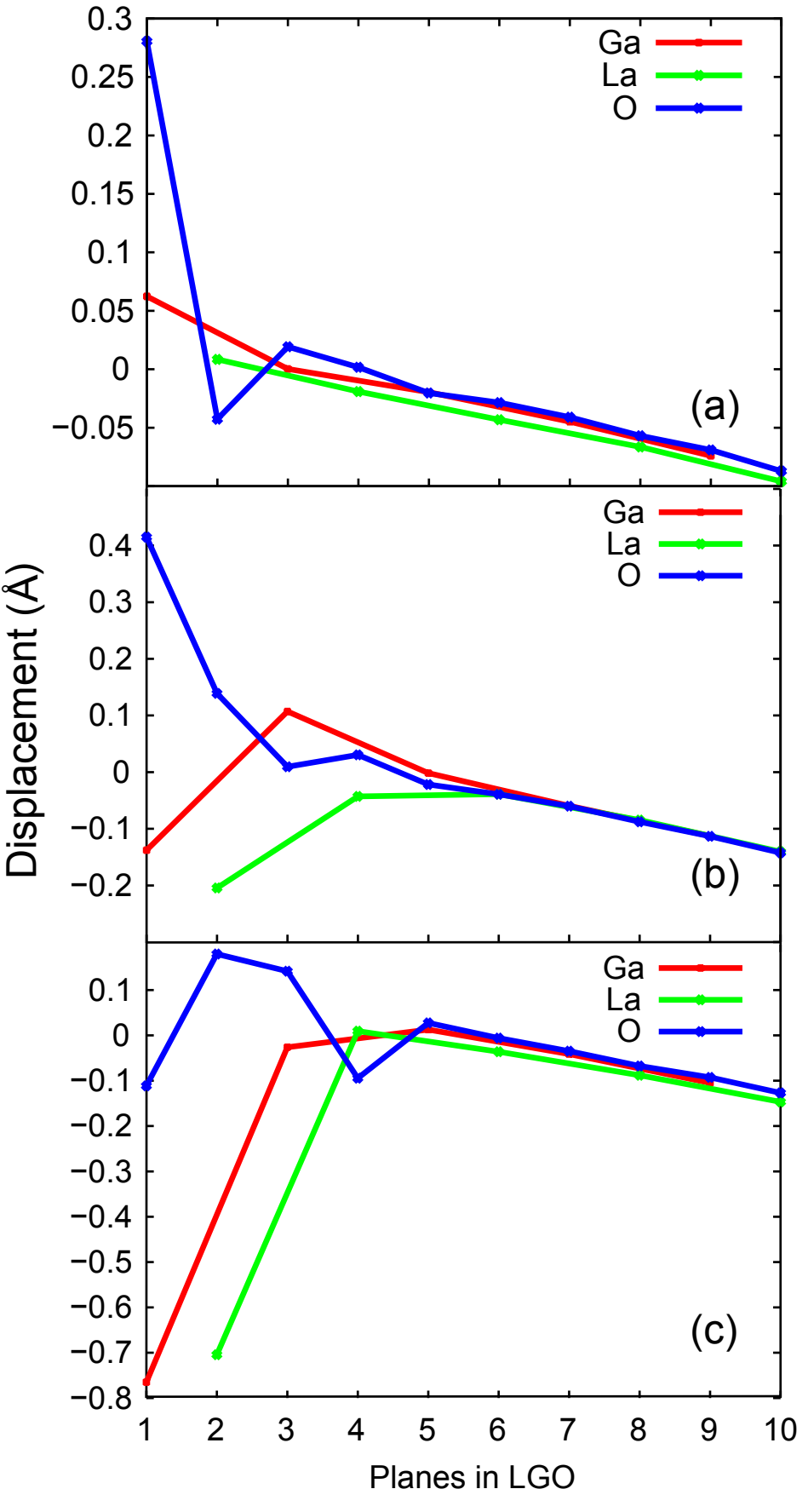
Ga
La
O
(a)
(b)
(c)
Displacement (Å)
Planes in LGO
0.3
0.25
0.2
0.15
0.1
0.05
0
−0.05
0.4
0.3
0.2
0.1
0
−0.1
−0.2
−0.3
−0.4
−0.5
−0.6
−0.7
−0.8
1
2
3
4
5
6
7
8
9
10

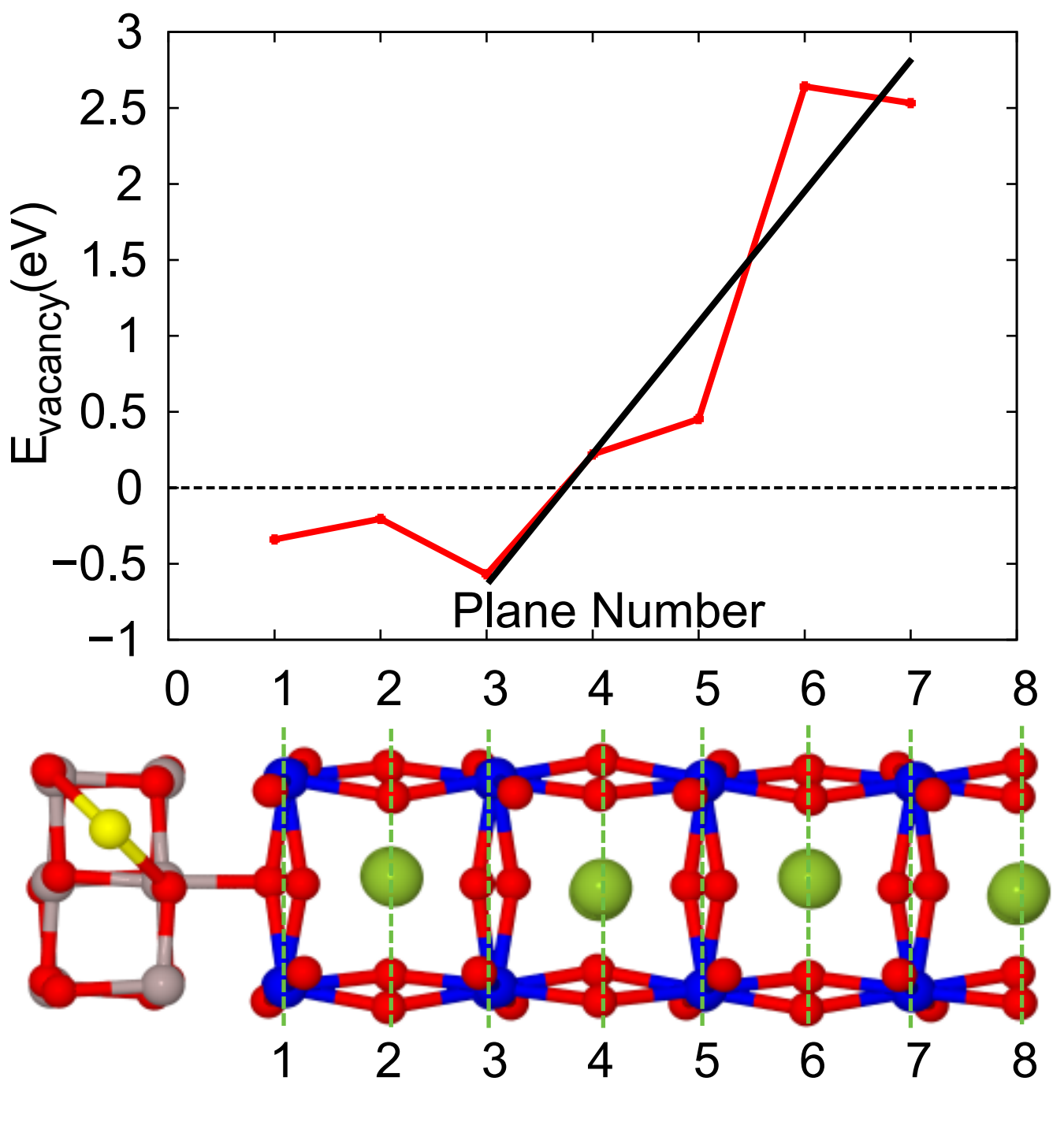
3
2.5
2
1.5
1
0.5
0
−0.5
−1
$E_{vacancy}$(eV)
Plane Number
0
1
2
3
4
5
6
7
8
1
2
3
4
5
6
7
8

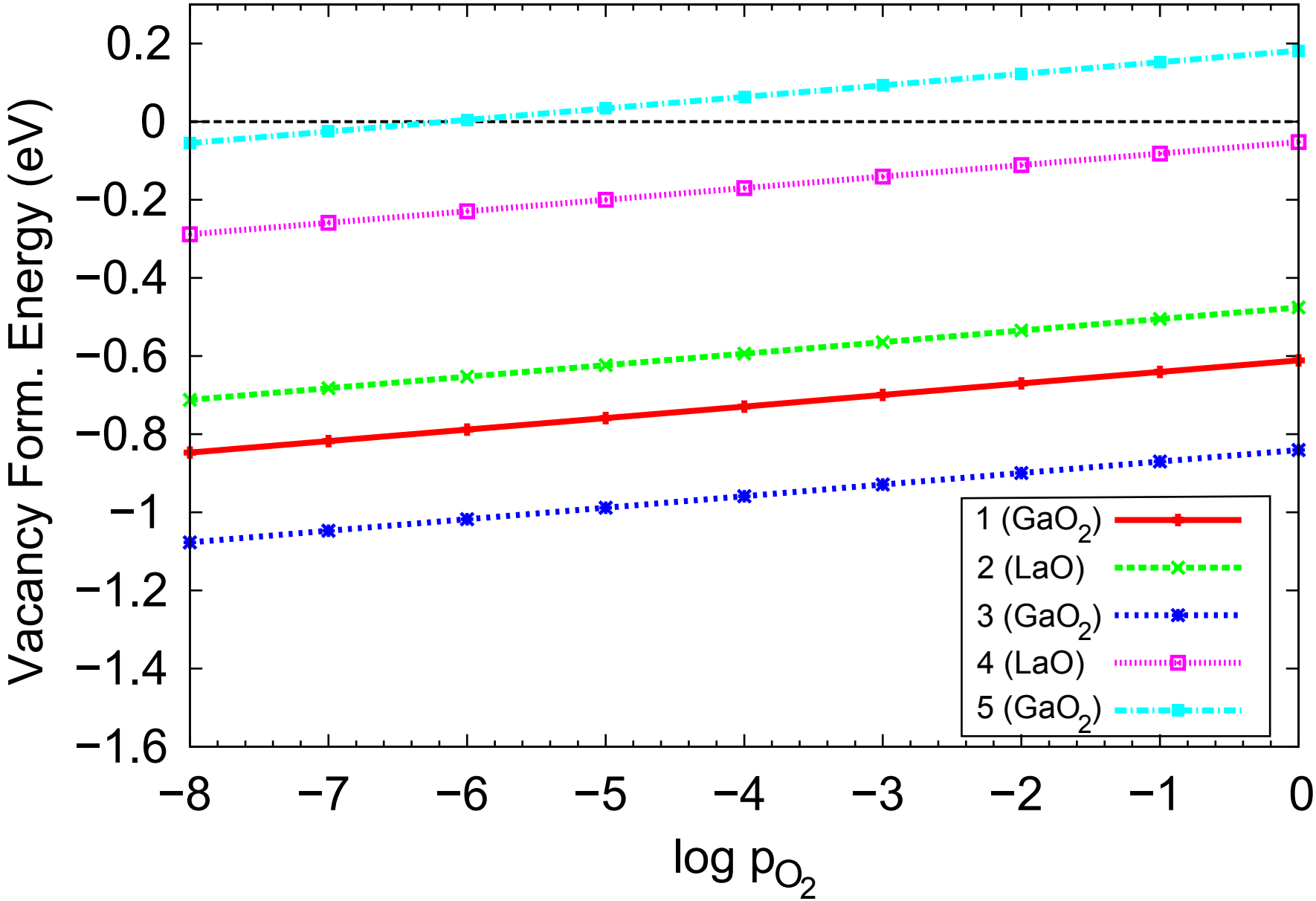
Vacancy Form. Energy (eV)
0.2
0
−0.2
−0.4
−0.6
−0.8
−1
−1.2
−1.4
−1.6
−8
−7
−6
−5
−4
−3
−2
−1
0
log p_{O_2}
1 (GaO_2)
2 (LaO)
3 (GaO_2)
4 (LaO)
5 (GaO_2)

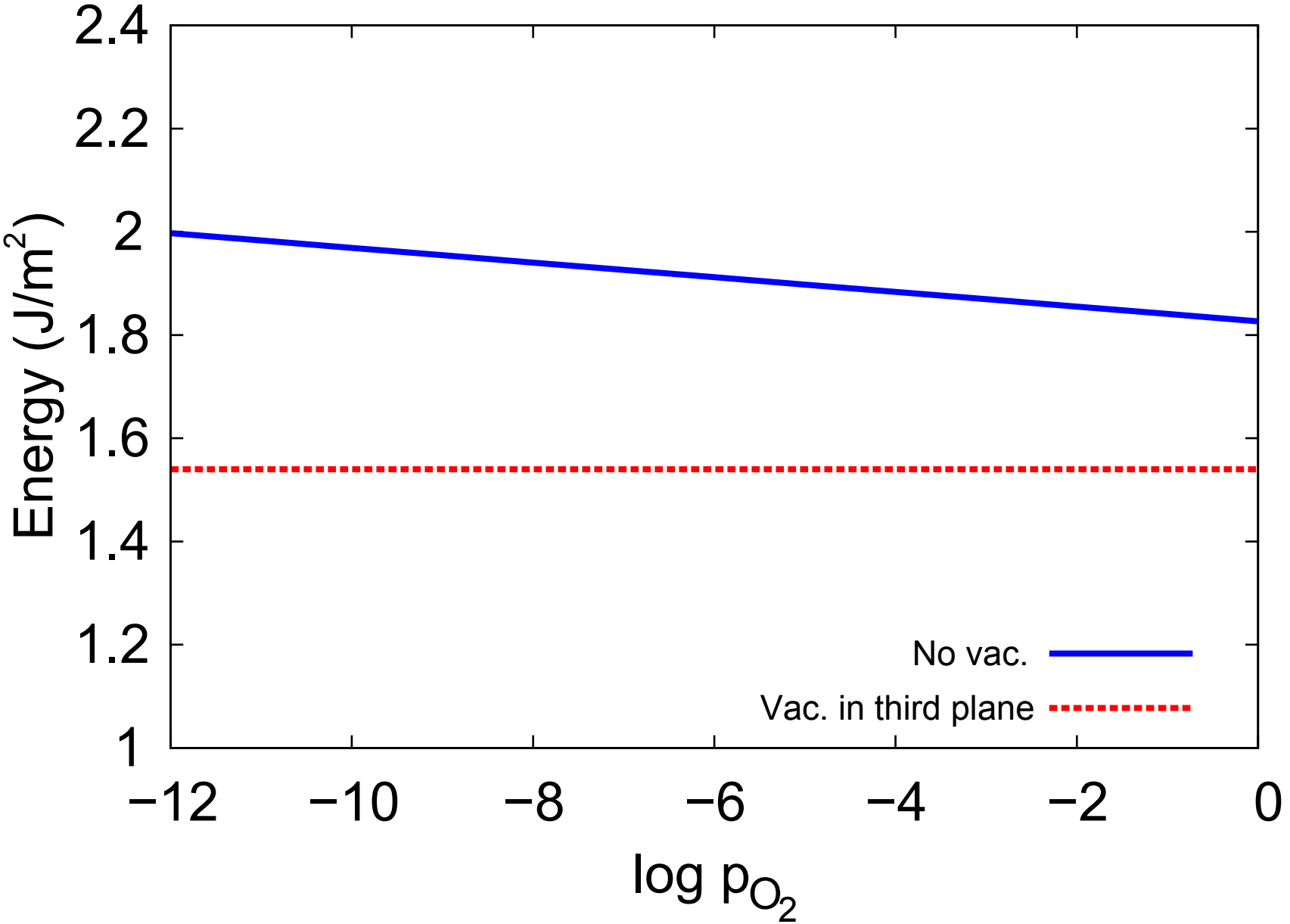
2.4
2.2
2
1.8
1.6
1.4
1.2
1
Energy (J/m^2)
−12
−10
−8
−6
−4
−2
0
log p_{O_2}
No vac.
Vac. in third plane

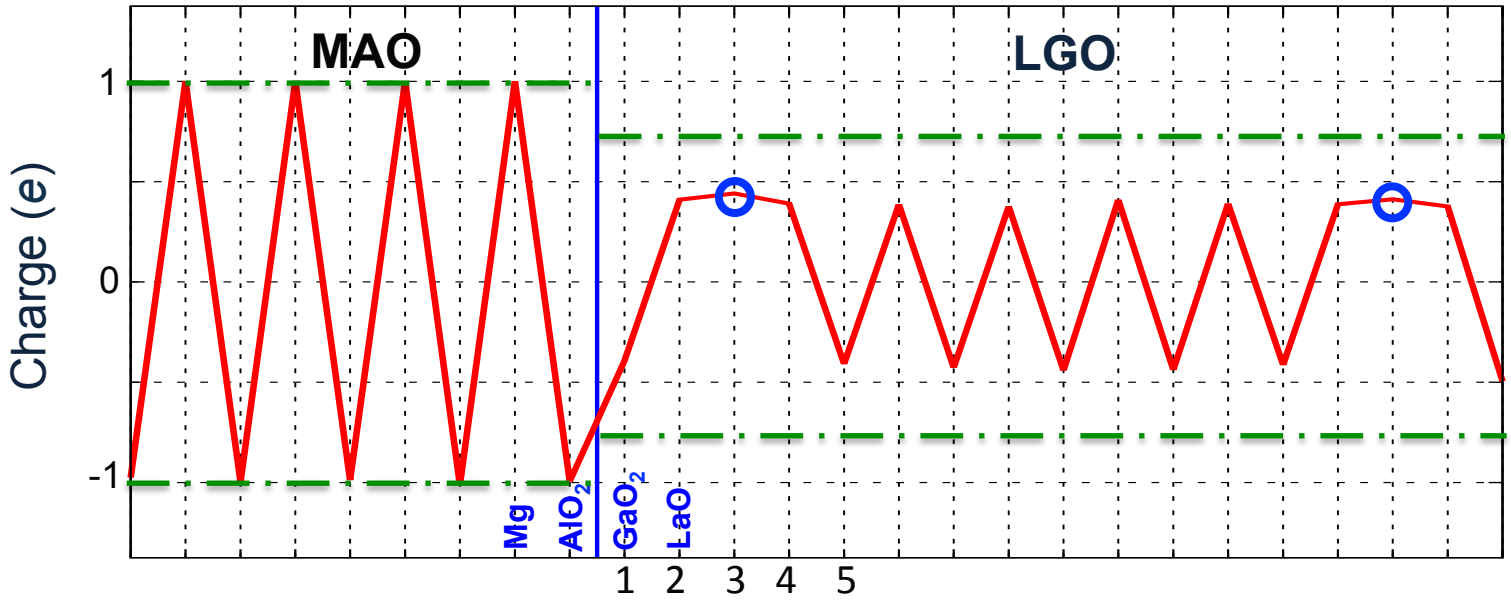
MAO
LGO
Charge (e)
1
0
-1
Mg
AlO2
GaO2
LaO
1
2
3
4
5

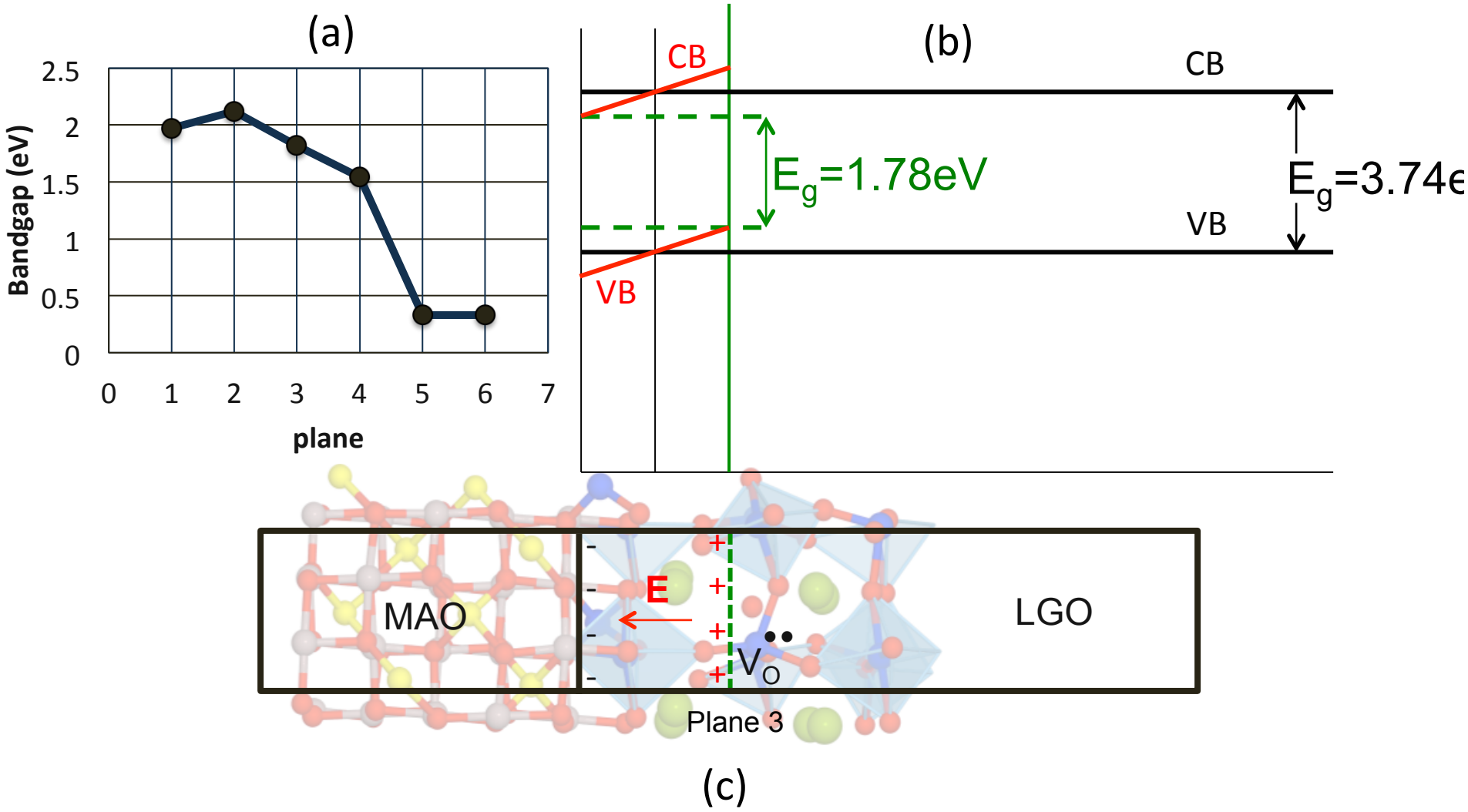
(a)
Bandgap (eV)
2.5
2
1.5
1
0.5
0
0 1 2 3 4 5 6 7
plane
(b)
CB
VB
E_g=1.78eV
CB
VB
E_g=3.74e
MAO
LGO
E
V_O
Plane 3
(c)

(a)

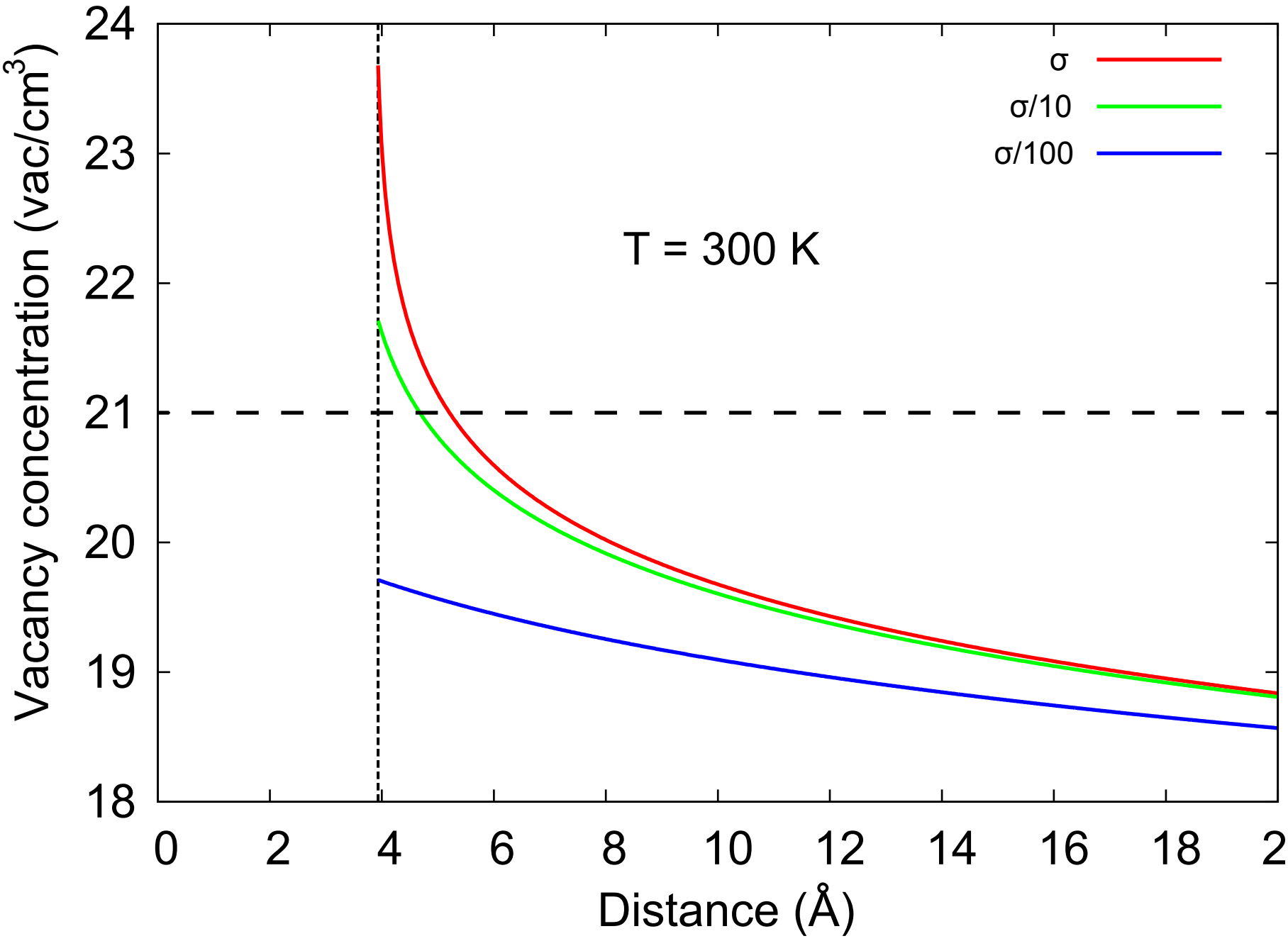
Vacancy concentration (vac/cm^3)
24
23
22
21
20
19
18
σ
σ/10
σ/100
T = 300 K
0
2
4
6
8
10
12
14
16
18
20
Distance (Å)

(b)

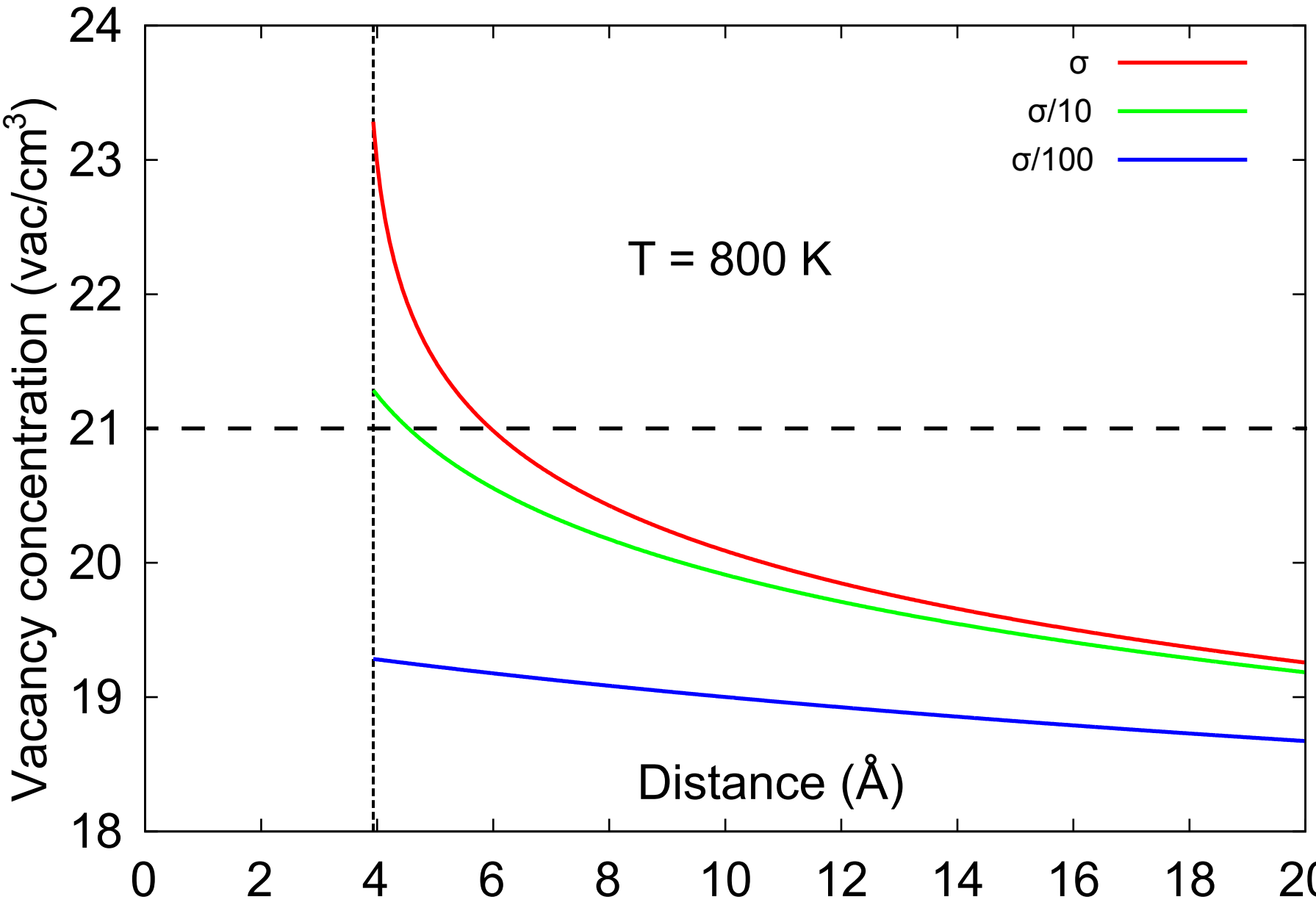
Vacancy concentration (vac/cm^3)
24
23
22
21
20
19
18
σ
σ/10
σ/100
T = 800 K
Distance (Å)
0
2
4
6
8
10
12
14
16
18
20

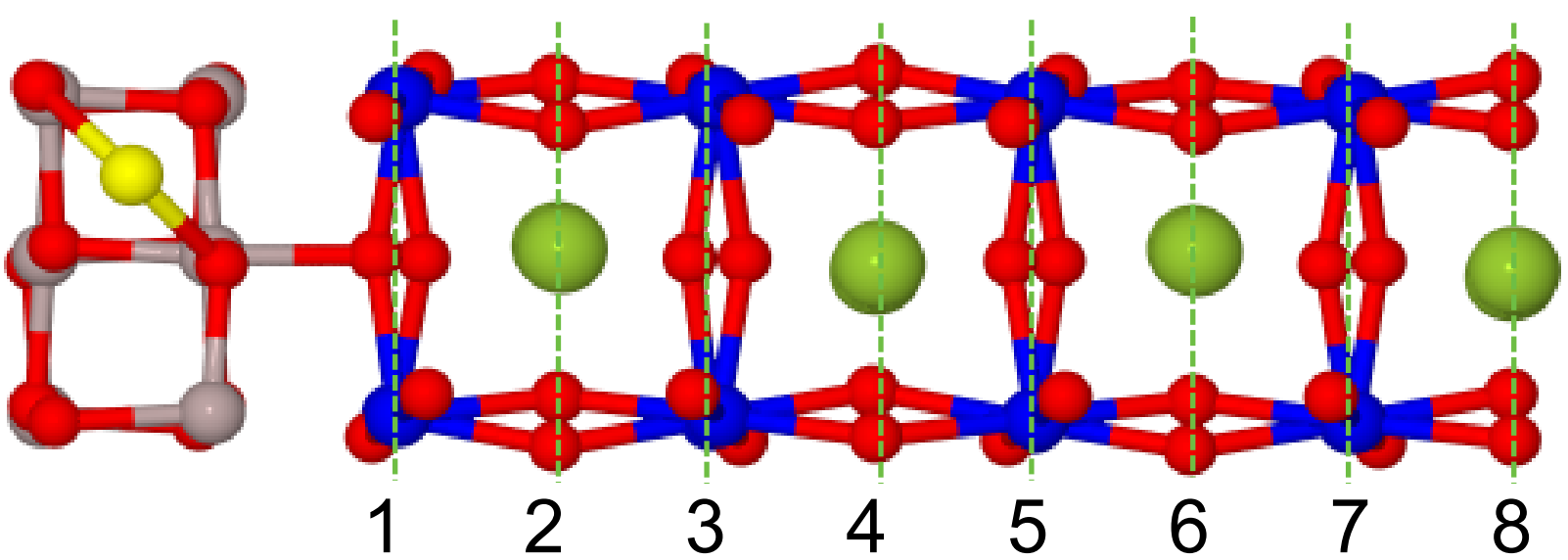
1
2
3
4
5
6
7
8